

11-2017

Adaptive Evolution under Extreme Genetic Drift in Oxidatively Stressed *Caenorhabditis elegans*

Stephen Fuller Christy
Portland State University, stephenfchristy@gmail.com

Riana I. Wernick
Oregon State University


Michael James Lue
Portland State University, hikari005@gmail.com

Griselda Velasco
Portland State University

Dana K. Howe
Oregon State University

See next page for additional authors

Follow this and additional works at: https://pdxscholar.library.pdx.edu/bio_fac

 Part of the [Biology Commons](#)

Let us know how access to this document benefits you.

Citation Details

Christy, S. F., Wernick, R. I., Lue, M. J., Velasco, G., Howe, D. K., Denver, D. R., & Estes, S. (2017). Adaptive evolution under extreme genetic drift in oxidatively stressed *Caenorhabditis elegans*. *Genome biology and evolution*, 9(11), 3008-3022.

This Article is brought to you for free and open access. It has been accepted for inclusion in Biology Faculty Publications and Presentations by an authorized administrator of PDXScholar. Please contact us if we can make this document more accessible: pdxscholar@pdx.edu.

Authors

Stephen Fuller Christy, Riana I. Wernick, Michael James Lue, Griselda Velasco, Dana K. Howe, Dee R. Denver, and Suzanne Estes

Adaptive Evolution under Extreme Genetic Drift in Oxidatively Stressed *Caenorhabditis elegans*

Stephen F. Christy^{1,†}, Riana I. Wernick^{2,†}, Michael J. Lue¹, Griselda Velasco¹, Dana K. Howe², Dee R. Denver², and Suzanne Estes^{1,*}

¹Department of Biology, Portland State University

²Department of Integrative Biology, Oregon State University

[†]These authors contributed equally to this work.

*Corresponding author: E-mail: estess@pdx.edu.

Accepted: October 21, 2017

Data deposition: This project has been deposited in the SRA database under accession number SRP069774.

Abstract

A mutation-accumulation (MA) experiment with *Caenorhabditis elegans* nematodes was conducted in which replicate, independently evolving lines were initiated from a low-fitness mitochondrial electron transport chain mutant, *gas-1*. The original intent of the study was to assess the effect of electron transport chain dysfunction involving elevated reactive oxygen species production on patterns of spontaneous germline mutation. In contrast to results of standard MA experiments, *gas-1* MA lines evolved slightly higher mean fitness alongside reduced among-line genetic variance compared with their ancestor. Likewise, the *gas-1* MA lines experienced partial recovery to wildtype reactive oxygen species levels. Whole-genome sequencing and analysis revealed that the molecular spectrum but not the overall rate of nuclear DNA mutation differed from wildtype patterns. Further analysis revealed an enrichment of mutations in loci that occur in a *gas-1*-centric region of the *C. elegans* interactome, and could be classified into a small number of functional-genomic categories. Characterization of a backcrossed four-mutation set isolated from one *gas-1* MA line revealed this combination to be beneficial on both *gas-1* mutant and wildtype genetic backgrounds. Our combined results suggest that selection favoring beneficial mutations can be powerful even under unfavorable population genetic conditions, and agree with fitness landscape theory predicting an inverse relationship between population fitness and the likelihood of adaptation.

Key words: adaptation, complex I, electron transport chain, mitochondrial dysfunction, mutation accumulation, sign epistasis.

Introduction

In agreement with predictions of Fisher's geometric model of adaptation (Fisher 1930), experimental evidence confirms that new mutations with measurable effects reduce the fitness of well-adapted genotypes (Lynch et al. 1999; Kondrashov and Kondrashov 2010). Original theoretical treatments of the threat to population survival posed by such mutations assumed that they affected fitness independently of genetic or environmental background and that little or no opportunity for reversion or other types of beneficial mutations existed (Lynch et al. 1993, 1995; Lande 1994). Empirical study suggests that both assumptions were wrong: beneficial mutations arise more frequently than originally appreciated

(Joseph and Hall 2004; Hall et al. 2008; Achaz et al. 2014) and the most readily harmful mutations—those with moderate fitness effects—may be rare (Estes et al. 2004; Katju et al. 2015). Furthermore, individual mutational effects can be highly dependent upon their environmental and genomic contexts (Lenski and Travisano 1994; Burch and Chao 1999; Elena and Lenski 2001; Maisnier-Patin et al. 2002; Rokyta et al. 2002; Estes and Lynch 2003; Remold and Lenski 2004; Wang et al. 2009, 2013), with a potentially large supply of compensatory epistatic mutations available to partially ameliorate the effects of previously acquired deleterious mutations. Indeed, adaptive landscape theory predicts that the probability of improvement increases with the distance

© The Author 2017. Published by Oxford University Press on behalf of the Society for Molecular Biology and Evolution.

This is an Open Access article distributed under the terms of the Creative Commons Attribution Non-Commercial License (<http://creativecommons.org/licenses/by-nc/4.0/>), which permits non-commercial re-use, distribution, and reproduction in any medium, provided the original work is properly cited. For commercial re-use, please contact journals.permissions@oup.com

of a population's mean fitness from a theoretical optimum, and that maladapted populations can access a greater fraction of beneficial mutations than well-adapted ones (Fisher 1930; Whitlock and Otto 1999; Poon and Otto 2000; Tenaillon 2014). In other words, the mutational distribution of fitness effects will depend upon how well adapted a population is (Martin and Lenormand 2006, 2015; Chevin et al. 2010). Another prediction is that small-effect beneficial mutations exist in greater supply than mutations of larger effect (Orr 1998); it follows that adaptive evolution in small populations (with fewer genomes available for mutation) will primarily be driven by fixation of small-effect mutations, whereas larger populations can adapt more quickly by fixing fewer large-effect mutations. These predictions have largely been borne out by data from studies with microbes (Burch and Chao 1999; Sanjuan et al. 2004; Perfeito et al. 2007; Silander et al. 2007; Barrick et al. 2010; Hietpas et al. 2013; Wang et al. 2013), although important exceptions exist (Miller et al. 2011). Studies in complex eukaryotes are still lacking (but see Stearns and Fenster 2016), which is problematic given the potential importance of organismal complexity and pleiotropy in determining real evolutionary outcomes (Orr 2000).

Laboratory mutation-accumulation (MA) experiments allow the impact of mutation to be distinguished from that of other evolutionary forces affecting rates of molecular evolution. Selection is rendered inefficient to the maximum extent possible by maintaining replicate lineages derived from a common ancestral genotype by clonal reproduction, self-fertilization, or extreme inbreeding across many generations, during which time MA lines accumulate and fix independent sets of mutations (Halligan and Keightley 2009; Teotónio et al. 2017). The vast majority of these experiments have initiated MA lines from wildtype ancestral strains that have undergone a period of laboratory domestication and are thus well adapted to laboratory conditions. Although we are aware of no MA experiments using extremely low-fitness ancestors, modifications to the standard MA design have included initiating MA lines from moderately low-fitness ancestors (Sharp and Agrawal 2012) and specific mutant genotypes for the purpose of revealing the effects of deficiencies in DNA repair pathways (Estes et al. 2004; Denver et al. 2006) and mitochondrial functioning (Joyner-Matos et al. 2011). Several MA experiments have now been combined with high-throughput sequencing to provide direct estimates of the average per-generation rate of mutations arising in nuclear genomes along with detailed analyses of their molecular spectra and patterns of bias (Lynch et al. 2008; Denver et al. 2009, 2012; Keightley et al. 2009; Ossowski et al. 2010; Lee et al. 2012; Saxer et al. 2012; Heilbron et al. 2014). When MA line fitness is evaluated, the near universal outcome is one of reduced mean fitness and increased among-line variance for fitness, consistent with mutations having predominantly deleterious effects. A notable exception is the study of

Shaw et al. (2000, 2002), which estimated that half of the mutations accumulated in MA lines of *Arabidopsis thaliana* were beneficial (Shaw et al. 2002)—a result later supported by Rutter et al. (2010, 2012). Shaw et al. (2000) originally suggested that intraindividual selection (e.g., differential cell lineage growth) may have contributed to this result. It would of course be difficult to experimentally minimize or control selection at this level, but by confining our attention to individual-level selection, we may underestimate the power of beneficial mutation to sustain the genetic health and fitness of populations.

The mitochondrial electron transport chain (ETC) offers a compelling framework for studying the endogenous factors that influence mutation. Because the mitochondrial ETC is vital for energy metabolism in all complex life and is thus highly conserved, it is an ideal system for studying the impact of deleterious mutation. Since proper ETC functioning relies on the maintenance of favorable mitonuclear epistatic interactions (Blier et al. 2001; Dowling et al. 2008), it is also an excellent system for addressing the role of epistasis in maintaining population fitness. The mitochondrial ETC also generates reactive oxygen species (ROS) as a byproduct of cellular metabolism (Murphy 2009). ROS are important cell signaling molecules (Mittler et al. 2011), but high ROS levels (e.g., resulting from mitochondrial dysfunction) have long been hypothesized to be mutagenic, especially for mtDNA genomes owing to their proximity to the site of production (Hsieh et al. 1986; Demple and Harrison 1994; Cooke et al. 2003). Recent work fails to implicate oxidative stress in somatic mtDNA mutation (Ameur et al. 2011; Yu et al. 2013; Itsara et al. 2014); however, the question of whether ROS are an important contributor to heritable germline mutation remains understudied.

Here, we build upon our previous work to provide a comprehensive, integrative assessment of the impact of mitochondrial dysfunction on nuclear DNA (nDNA) variation and phenotypes related to fitness and physiology. As described in Wernick et al. (2016), which reported on mitochondrial DNA mutation processes, we performed a MA experiment using a mitochondrial ETC-deficient genotype of *C. elegans*, *gas-1(fc21)*, as the ancestor. We phenotyped replicate MA lines initiated from this mutant and applied Illumina MiSeq technology to analyze the nuclear genomes of a subset of these lines. As before, we compare our findings to those from a previous MA study initiated from a wildtype *C. elegans* ancestor (Baer et al. 2005). Bioinformatic approaches identified novel, putatively beneficial mutations fixed within MA lines; a subset of these was characterized to determine the contribution to surprising patterns of fitness and phenotypic evolution observed here.

Materials and Methods

Strains

This study utilized MA lines generated from a *gas-1* mutant strain of *C. elegans*. The *gas-1(fc21)* allele is a single basepair

missense mutation (Kayser et al. 1999) associated with deleterious phenotypes including: reduced fecundity, reduced complex I-dependent metabolism (Kayser et al. 2004), hypersensitivity to oxidative stress owing to increased ROS production (Kayser et al. 2001, 2004), and low ATP levels relative to wildtype (Hartman et al. 2001; Kayser et al. 2001, 2004; Lenaz et al. 2006). The *gas-1* mutant, derived from ethyl methanesulfonate (EMS) mutagenesis (Kayser et al. 1999), was obtained from the *Caenorhabditis* Genetics Center (University of Minnesota) and repeatedly backcrossed to N2 in an attempt to create an isogenic mutant strain. As detailed in Wernick et al. (2016), which reported on the mitochondrial DNA mutation processes within the same MA lines, offspring of a single *gas-1* (*fc21*) hermaphrodite were then used to initiate 48 MA lines, maintained for an average of 43 generations (range: 35–47). Failed bottlenecks occasionally resulted from hermaphrodite sterility or death prior to reproduction; in this event, a sibling from the same generation was chosen from a backup plate to initiate the next generation. An MA line was considered extinct when it could not be reconstituted in this way. A subset of five *gas-1* MA lines was selected at random for whole-genome sequencing and additional phenotypic analyses. We also utilized data from a previous analysis of MA lines generated from a wildtype N2 strain, which were evolved in the manner described earlier for a maximum of 250 generations (Baer et al. 2005). Namely, *gas-1* MA results were compared with those from a subset of five N2 MA lines for which genome sequence (Denver et al. 2009, 2012) and phenotypic data (Denver et al. 2009; Joyner-Matos et al. 2013; Andrew et al. 2015) were available.

Life History Assays and Data Analysis

We assayed nematode life-history and analyzed the resulting data following established methods (Joyner-Matos et al. 2011). Owing to difficulty in working with the poorly performing *gas-1* MA lines, life-history assays were conducted in four blocks in which different subsets of *gas-1* MA lines were assessed alongside N2 and *gas-1* ancestral (hereafter “*gas-1* G0” for generation 0) controls. A fifth and sixth block were conducted to increase the sample size of the five *gas-1* MA lines selected for whole genome sequencing (below). Specifically, we measured daily offspring production for the *gas-1* MA lines, *gas-1* G0 and N2 strains; we also recorded the number of unhatched and presumably unviable eggs, easily distinguished from unfertilized eggs under a light microscope. Data were used to calculate mean absolute (total reproductive output, W) and relative fitness (ω) of the *gas-1* mutant compared with N2, and of each *gas-1* MA line compared with the *gas-1* G0 ancestor. Relative fitness of each individual was computed as: $\omega = \sum e^{-rx} l(x) m(x)$, where $l(x)$ is the number of worms surviving to day x , $m(x)$ is the fecundity at day x , and r is the mean intrinsic population growth rate of the assay-specific N2 or *gas-1* G0 control as appropriate. The

latter was calculated by solving Euler’s equation for r from the equation $\omega = \sum e^{-rx} l(x) m(x) = 1$ using an average value of $l(x) m(x)$ for each block-specific control. We used $x = 4.75$ on the first reproductive day (c.f., Vassilieva et al. 2000).

To determine the impact of MA on evolution of the above phenotypes, the per generation change in the mean, ΔM , of each trait was estimated as the generalized linear regression coefficient of trait value scaled as a fraction of the block-specific *gas-1* G0 mean on line-specific MA generation number. For the MA lines, within- and among-line components of variance were calculated using restricted maximum likelihood (REML) with variance estimates constrained to be nonnegative (except for when calculating confidence intervals). We tested the model *trait mean* = $\mu + \text{block} + \text{MA line}(\text{block}) + \text{parent}[\text{MA line}(\text{block})] + \varepsilon$, wherein all effects are random—and *MA line(block)* represents among-line (genetic) variance and ε represents the within-line (environmental) component of variance, V_E . A frequency distribution of *gas-1* MA line fitness relative to *gas-1* G0 was created using least squares means for the *gas-1* MA lines derived from the *MA line(block)* term using the expected mean squares (EMS) method as applied in JMP12 (SAS). For N2 and *gas-1* G0 control lines, we tested the model *trait mean* = $\mu + \text{block} + \text{parent}(\text{block}) + \varepsilon$, wherein all effects are random and *parent(block)* represents among-line (or pseudoline) variance. Second, the per-generation change in genetic variance owing to MA, the mutational variance V_M , was calculated for each trait as the difference in the among-line components of variance of the *gas-1* G0 control and the MA lines divided by $2t$, where t = the maximal number of MA generations. The per generation change in among-line variance, V_b , was calculated for the *gas-1* MA lines by dividing the among line variance for each line by the average number of generations, 42.8.

Steady-State ROS and ATP Levels

Prior to all experiments, strains were allowed to recover from freezing for two generations at 20 °C on Nematode Growth Medium-Lite (NGML) plates containing 20 $\mu\text{g/ml}$ streptomycin and seeded with *Escherichia coli* OP50-1. Lines were age synchronized by standard bleach treatment prior to each assay. We quantified in vivo steady-state ROS levels of the five *gas-1* MA lines compared with N2 and *gas-1* G0 strains using established fluorescence microscopy methods (Hicks et al. 2012; Joyner-Matos et al. 2013; Smith et al. 2014). ROS levels of the five sequenced N2 MA lines were previously reported (Joyner-Matos et al. 2013). We quantified ATP content for four to five independent samples from each of the five N2 and *gas-1* MA lines compared with N2 and *gas-1* G0 strains following methods adapted from Van Raamsdonk et al. (2010) and Yang and Hekimi (2010). For each sample, roughly 200 age-synchronized young adult worms were washed and worm cuticles were broken via successive freeze-thaw cycles. Samples were boiled for 15 min, sonified (20% amplitude,

twice for 12 s), and centrifuged at 10,000×g for 12 min. About 90 μl of supernatant was used to quantify ATP levels with a luminescence ATP detection kit (Invitrogen, Carlsbad, CA) and a TECAN Infinite M200 Pro plate reader (Tecan, Männedorf, Switzerland). ATP measurements were normalized by protein content measured with a Pierce BCA Protein Assay Kit (Thermo Fisher Scientific, Waltham, MA).

Illumina MiSeq Read Mappings and Analyses

Whole-genome sequencing was conducted for five randomly chosen *gas-1* MA lines, N2 and the backcrossed *gas-1* G0. Samples were prepared from first larval (L1) stage nematodes as described in (Wernick et al. 2016). Following each Illumina MiSeq run, reads were aligned to the *C. elegans* genome (version WS242) using CLC Genomics Workbench (CLC Bio-Qiagen, Aarhus, Denmark). All reads were paired-end (2×150 bp) and mapped using the following parameters: no masking, mismatch cost = 2, insertion cost = 3, deletion cost = 3, length fraction = 0.98, read fraction = 0.98, global alignment = no, nonspecific match handling = map randomly. Illumina data were deposited in the SRA database under accession number SRP069774.

Characterization of *gas-1* G0 Genetic Background

Two potential sources of genetic difference between the *gas-1* G0 and N2 progenitor strains are: (1) mutations resulting from the EMS mutagenesis employed to create the original *gas-1* mutant, and (2) spontaneous mutations fixed during the ten generations of backcrossing. The majority of mutations from the first source should have been eliminated during the ten generations of backcrossing *gas-1* to N2 males, but some EMS-induced mutations, particularly those closely linked to the *gas-1* locus, may have remained. *C. elegans* experiences base substitutions at the rate of approximately two per generation (Denver et al. 2004), meaning that roughly 20 mutations were expected to have accumulated during the backcrossing process. All single-basepair mutations in *gas-1* G0 were identified as sites that differed from the *C. elegans* reference genome (WS242) and were not present in our N2 strain. To eliminate false positives resulting from sequencing artifacts, candidate mutations for which coverage was less than the average coverage of *gas-1* candidate SNPs (18×) were omitted. Additionally, the following criteria were applied: (1) 100% of reads indicated a single nonreference base, (2) at least one read was present from both the reverse and forward strand, and (3) reads in a given direction varied upon start/end positions. Mutations of the six possible substitution types were counted in a chromosome-specific manner. Characteristics of *gas-1* G0 mutations meeting the above criteria were compared with those published for N2 (Denver et al. 2012). χ^2 tests were applied to test for significance.

Identification and Characterization of *gas-1* MA Line Mutations

Candidate SNPs in *gas-1* MA lines were identified as variants from the *C. elegans* reference genome (WS242) and our N2 lab strain. Each MA line was also surveyed for retention or loss of SNPs identified in *gas-1* G0. To eliminate false positives, we applied the aforementioned criteria and required at least 5-fold coverage. Lastly, we only considered mutations found in one line to eliminate false positives associated with cryptic heterozygosity or paralogy following our previous approaches (Denver et al. 2009, 2012).

Mutation Rate Analysis

The nuclear mutation rate was calculated as previously described (Denver et al. 2009) from pooled *gas-1* MA lines using the equation $\mu_{bs} = m / (LnT)$ where μ_{bs} is the base substitution rate (per nucleotide site per generation), m is the number of observed mutations, L is the number of MA lines, n is the number of nucleotide sites, and T is the time in generations. Values for n reflect the total number of base pairs surveyed that met the criteria for consideration of a possible mutation site. Conditional rate estimates for the six possible mutation types (A: T → G: C, G: C → A: T, A: T → C: G, G: C → T: A, A: T → T: A, and G: C → C: G) were also determined in a non-strand specific manner using the pooled *gas-1* MA line mutations. Standard errors for these estimates were approximated as $[\mu_{bs} / (nT)]^{1/2}$. We compared observed conditional rate estimates in the *gas-1* MA lines to published values for N2 MA lines (Denver et al. 2012).

Gene Ontology Enrichments

We used GoMiner (Zeeberg et al. 2003, application build 457) and the GO MySQL Database (MySQL 3.7.13, Oracle Corporation, Cupertino, CA; GO database build 2016-06-07, geneontology.org) to calculate gene ontology (GO) enrichments for genes in the *gas-1* interactome and all nDNA SNPs that arose within protein coding regions of *gas-1* MA and the N2 MA lines within three functional domains—biological process, cellular component, and molecular function. GoMiner reports a two-sided Fisher's exact P value based upon the number of genes in a category and a false discovery rate (FDR)-corrected P value for multiple testing (Zeeberg et al. 2005); however, the FDR can be overly conservative when the sample size or number of discoveries is small; that is, <100 (Zeeberg et al. 2005; Tong and Zhao 2008), so we based interpretations on results of the Fisher's exact tests with $\alpha = 0.05$. We then determined which broader-level functional "GO slim" categories, as defined by the GO Consortium (Version 1.2, 2012-09-21, geneontology.org), were enriched using CateGORizer (Hu et al. 2008), which classifies enriched GO terms into their respective GO slim categories, giving a coarser-scale overview of enrichment

patterns. GO slim categories were then checked against the GoMiner output to assess statistical significance.

Interactome Analysis of *gas-1* and N2 MA Line Mutations

Following our previous approach (Denver et al. 2010), GeneOrienteer version 2.25 (Zhong and Sternberg 2006) was used to construct an interactome, a list of genes predicted to interact with a gene of interest (*gas-1*), and determine the extent to which mutated MA line genes showed membership within this network. We first queried the entire *C. elegans* interactome to determine the interactions involving *gas-1*. The query returned 181 genes predicted to “directly” interact with *gas-1* within one degree. We then queried this smaller interactome to identify genes predicted to interact within two degrees of *gas-1*. We refer to the comprehensive list of first- and second-degree *gas-1* interacting genes, totaling 4,189, as the “*gas-1* centric interactome.” We next identified all genic mutations within the *gas-1* and N2 MA line sets that were members of the *gas-1*-centric interactome and used Monte Carlo Maximum Likelihood simulations to assess the probability of observing the results by chance. Twenty-three mutations (the number of genic mutations discovered in *gas-1* MA lines) were randomly generated using a simulation written in Python. This simulation was repeated for 1,000 iterations, and the average and standard deviation of the number of mutations occurring within the *gas-1* centric interactome were calculated. This simulation was repeated for N2 with the exception that 59 mutations, the number of genic mutations discovered within N2 MA lines (Denver et al. 2012), were randomly generated.

Isolation and Characterization of Candidate Beneficial Mutations from MA431

Because results of the above analyses indicated that some degree of adaptive evolution had occurred in the *gas-1* MA lines, we aimed to characterize candidate beneficial or compensatory SNPs that arose within one particular line. Line MA341 was chosen for analysis as it was found to contain SNPs affecting genes identified by the GO and interactome analyses and/or with known function—namely, *rheb-1*, *daf-2*, and *sel-2*, all of which reside on chromosome III. Toward this goal, MA431 was backcrossed to N2 following the same approach used to generate the *gas-1* G0 strain. At each generation, DNA was extracted from the parental MA431 hermaphrodite ($n = 30\text{--}44$) for PCR and Sanger DNA sequencing at three SNP locations within the *rheb-1*, *daf-2*, and *sel-2* genes. Offspring from hermaphrodites retaining at least one of these SNPs were used in the next round of crossing. Although our aim was to isolate each chromosome III SNP individually, we were unsuccessful at maintaining strains that did not contain all three (see Results for MA431 SNP linkage).

After seven rounds of backcrossing, hermaphrodites containing MA431 mutations were allowed to self and tested to find homozygotes, resulting in a strain referred to hereafter as N2^{MA431}. Finally, the MA431 chromosome III homozygous mutant lines were crossed with our near-isogenic *gas-1* G0 strain and offspring allowed to self to produce a strain that contained only the chromosome III SNP mutations on the *gas-1* background, *gas-1*^{MA431}.

We performed a life-history assay as previously described for the N2^{MA431} and *gas-1*^{MA431} strains alongside N2 and *gas-1* G0 controls, which included 40 replicates of each strain. Selection coefficients of the MA431 SNPs on each genetic background were calculated as the difference in relative fitness between N2^{MA431} and N2 and between *gas-1*^{MA431} and *gas-1* G0. A Cox proportional hazards method was used to compare age-specific mortality of the N2^{MA431} and *gas-1*^{MA431} strains and their N2 and *gas-1* G0 controls, with *strain* and *parent(strain)* as main effects. Lastly, we quantified in vivo steady-state ROS and ATP levels of the N2^{MA431} and *gas-1*^{MA431} lines compared with N2 and *gas-1* G0 strains as previously described.

Results

Characterization of *gas-1* G0 Genetic Background

Bioinformatic analysis of the *gas-1* G0 strain identified 76 genetic differences relative to our N2 strain (supplementary fig. S1 and table S1, Supplementary Material online). The X-chromosome (where *gas-1* is located) harbored the majority, ~62%, of these mutations compared with 15.7% of the total mutations identified in the N2 MA lines (Denver et al. 2012)—a highly significant difference ($P < 0.00001$, χ^2 test). The *gas-1* G0 X-chromosome also experienced an increased proportion of G: C→A: T mutations compared with published N2 MA line results (80.9% vs. 23.5%; $P < 0.00001$, χ^2 test). Genome-wide, the *gas-1* G0 strain also showed a much higher proportion of G: C→A: T mutations compared with the published N2 value (61.8% vs. 33.3%; $P < 0.00001$, χ^2 test). All 76 background mutations present within *gas-1* G0 were retained within the sequenced MA lines (below).

gas-1 G0 Phenotypes

There were no significant effects of assay block on any life-history trait (not shown). As expected based on previous studies of the CGC *gas-1* strain (Morgan and Sedensky 1994; Kayser et al. 1999), our backcrossed *gas-1* G0 strain produced far fewer offspring than N2 (fig. 1 and table 1; supplementary table S2, Supplementary Material online), resulting in lower relative fitness ($t_{(148)} = 9.954$, $P < 0.0001$; table 1). *gas-1* G0 reproductive maturity and peak reproductive output were also delayed by a full day compared with N2 (fig. 1).

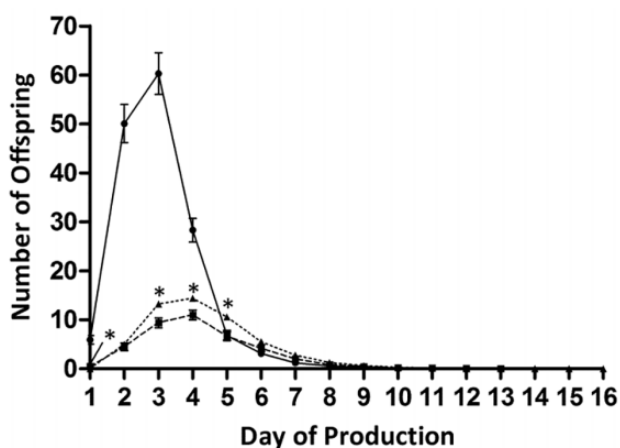


Fig. 1.—Reproductive schedules. Daily offspring production of N2 (solid line), *gas-1* G0 (dashed line, squares), and the combined *gas-1* MA lines (dashed line, triangles). Error bars are 1 SEM. Summary statistics are reported in supplementary table S2, Supplementary Material online.

Table 1

Summary Statistics for Fitness Traits

	<i>W</i>	ω
N2	151.6 ± 10.03	1.000 ± 0.053
<i>gas-1</i> G0	38.40 ± 3.277	0.225 ± 0.057
<i>gas-1</i> G0 ^a	38.40 ± 3.277	1.000 ± 0.085
<i>gas-1</i> MA ^a	50.58 ± 1.647	1.260 ± 0.058
ΔM (x 10 ⁻³)	127.9 ± 38.20	5.757 ± 1.317
<i>V_b</i> <i>gas-1</i> G0	76.74 ± 84.81	0.054 ± 0.059
<i>V_b</i> <i>gas-1</i> MA	5.191 ± 1.824	0.010 ± 0.004
<i>V_E</i> <i>gas-1</i> G0	628.6 ± 105.7	0.014 ± 0.002
<i>V_E</i> <i>gas-1</i> MA	20.58 ± 1.439	0.017 ± 0.001
<i>V_M</i>	-1.547	-0.004

NOTE.—All values are means ± 1 SEM.

^aFitness relative to *gas-1* G0; fitness is otherwise reported relative to N2.

W, absolute fitness; ω , relative fitness.

Potential for Selection during *gas-1* MA

Eight of the original 48 *gas-1* MA lines (16.7%) went extinct prior to the 50 generation cut-off, as compared with only one extinction among 48 MA lines initiated from N2 (2%) during 125 generations of evolution (Joyner-Matos et al. 2011). The frequency of failed bottlenecks occurring during the *gas-1* MA experiment, 14.2%, was twice that reported for the N2 MA lines, 7.1% (Joyner-Matos et al. 2011). Additionally, *gas-1* MA lines laid an increased number of fertilized but ultimately unhatched eggs compared with ancestral controls. The difference in unhatched egg counts among N2, *gas-1* G0 and MA groups ($F_{2, 677} = 8.9345$, $P < 0.0001$) was due to the *gas-1* MA line group having a small but significantly greater number of unhatched eggs (3.68 ± 0.31) than either *gas-1* G0 (1.51 ± 0.41) or N2 (1.09 ± 0.18) (Tukey HSD; $\alpha = 0.05$, $P < 0.01$). In contrast, the prevalence of “bagging” (where internal hatching of eggs kill the parent) in the MA

lines (8.2%) was indistinguishable from that in N2 (12.4%) or *gas-1* G0 (10.2%) (χ^2 test), and thus did not significantly impact MA line fitness.

gas-1 MA Life-History Evolution

gas-1 lines evolved higher average absolute and relative fitness during the MA process, leading to positive values for ΔM , the per generation change in mean phenotype (table 1). These differences were due to MA lines producing, on an average, significantly more offspring on days 1, 3, 4, and 5 of their reproductive period (fig. 1 and supplementary table S2, Supplementary Material online). Eighteen MA lines were the major contributors to this pattern; of the remaining 30 MA lines, 8 went extinct (above) and 22 exhibited unchanged or slightly reduced fitness relative to *gas-1* G0 (fig. 2).

As expected, phenotypic variance among ancestral N2 or *gas-1* G0 control lines did not differ from zero for absolute or relative fitness (table 1); within-line (environmental) variance estimates are shown in supplementary table S3, Supplementary Material online. Significant per-generation changes in among-line (genetic) variance, V_b , were detected for both fitness metrics in *gas-1* MA lines (table 1). However, point estimates for V_b were uniformly lower for *gas-1* MA lines compared with those for the *gas-1* G0 ancestor for both traits (table 1). If we had corrected for the (nonsignificant) among-(pseudo)line variance observed for the *gas-1* G0 control (c.f., Joyner-Matos et al. 2011), we would have detected no genetic variance for the MA lines. Accordingly, mutational variance, V_M , estimates are low and slightly negative for both traits (table 1). Finally, a roughly similar pattern of reduced variance was observed for V_E , the per-generation within-line variance, meaning that average MA line performance became more uniform compared with that of its ancestor.

gas-1 MA ROS and ATP

No significant block or interaction effects for either ROS or ATP were found when N2 and *gas-1* G0 control performance was modeled as a two-way ANOVA: $y = \mu + strain + block + strain * block + \epsilon$, where *block* and *strain * block* are random effects (not shown). *gas-1* G0 exhibited significantly higher ROS (supplementary fig. S2A, Supplementary Material online) and lower ATP (supplementary fig. S2B, Supplementary Material online) than N2. *gas-1* MA line ROS levels were significantly reduced compared with *gas-1* G0 and statistically indistinguishable (although higher) than wildtype levels (supplementary fig. S2A, Supplementary Material online). *gas-1* MA lines also exhibited lower amounts of within-line variance than *gas-1* G0, approaching levels observed for N2 (not shown). Average steady-state ATP levels in the *gas-1* MA lines were unchanged compared with *gas-1* G0; both *gas-1* G0 and its MA lines had significantly reduced

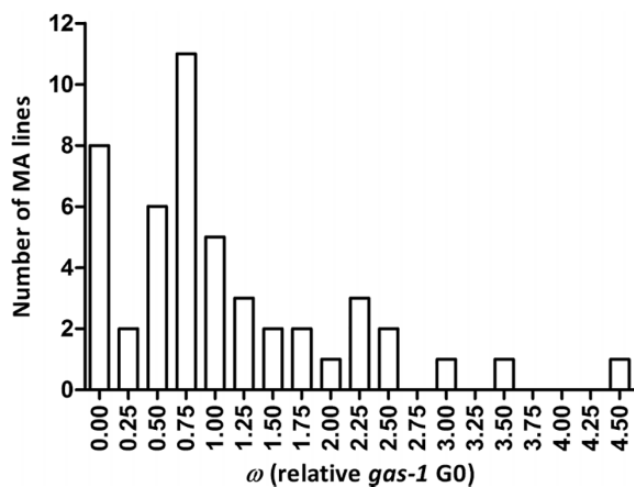


FIG. 2.—Frequency histogram of *gas-1* MA relative fitness. Histogram of the 48 *gas-1* MA lines' fitness (w) relative to *gas-1* G0 (equal to 1.0) using least squares means including the 8 *gas-1* MA lines that went extinct.

ATP levels compared with wildtype N2 (supplementary fig. S2B, Supplementary Material online).

Rates and Spectra of *gas-1* MA Line Mutations

Forty novel mutations were detected across the five sequenced *gas-1* MA lines (table 2); additionally, all 76 background mutations detected within *gas-1* G0 were retained by each MA line. Considering only the novel mutations that arose during MA, MA-line specific mutation numbers ranged from 5 to 11. The per-generation base-substitution mutation rate, $2.13 (\pm 0.34) \times 10^{-9}$, was statistically indistinguishable (within two SEM) from that previously reported for N2, $2.7 (\pm 0.40) \times 10^{-9}$ (Denver et al. 2009). The largest mutation class (16/40) was composed of G: C \rightarrow A: T transition events. Compared with estimates published for N2 MA lines (Denver et al. 2012), these events alone were substantially elevated in the *gas-1* MA lines (SEM values for N2 and *gas-1* MA G: C \rightarrow A: T conditional rates did not overlap; supplementary fig. S3, Supplementary Material online). There was no significant difference between the proportion of synonymous to nonsynonymous mutations between the *gas-1* MA and N2 MA values ($P = 0.92$, χ^2 test).

GO Term Enrichment

Supplementary file S1, Supplementary Material online, gives a complete accounting of GO enrichment results. No significantly enriched GO slim categories were shared between the *gas-1* MA and N2 MA line groups (supplementary file S1, Supplementary Material online and fig. 3A and B). For *gas-1* MA lines, two categories were significantly enriched: the biological process of transport and the cellular component of plasma membrane (fig. 3A). Four *gas-1* MA line genic

mutations were classified under both transport and plasma membrane; those in: *smf-3*, *daf-2*, *twk-3*, and *rheb-1* genes. In contrast, 12 GO slim categories were enriched in the N2 MA lines (fig. 3B). In addition to the lack of overlap between enriched *gas-1* and N2 MA line GO slim categories (fig. 3A and B), we found that all 12 GO slim categories enriched among N2 MA lines were also enriched in the entire *gas-1* interactome set (see below), which contained 80 significantly enriched GO slim categories. Conversely, transport was the only term enriched among both the *gas-1* MA line and *gas-1* interactome gene sets.

gas-1 Interactions

Of the 23 genic mutations (i.e., those discovered within exons or introns; table 2) found within sequenced *gas-1* MA lines, 8 were predicted to interact within 2-degrees of the *gas-1* gene (fig. 3C); 1 of these, *alh-2*—encoding a mitochondrial aldehyde dehydrogenase—was a direct interactor with *gas-1*. Simulations revealed that this number (eight) was higher than that expected by chance, 3.3 ($P = 0.005$, χ^2 test; supplementary fig. S4, Supplementary Material online), and in only 6 of the 1,000 iterations did eight or more mutations reside within this network. None of the 76 *gas-1* G0 background mutations was found within the interactome. Of the 59 genic mutations found within sequenced N2 MA lines, 12 were located within the *gas-1*-centric interactome. In contrast to the *gas-1* MA line result, this number was no different than that expected by chance, 8.4 ($P = 0.177$, χ^2 test; supplementary fig. S5, Supplementary Material online); 131/1,000 iterations saw at least 12 mutations located in genes predicted to interact within 2-degrees of *gas-1*.

MA431 SNP Linkage and Characterization

The above analyses revealed several notable SNPs to be contained within one *gas-1* MA line, MA431; we therefore sought to isolate and individually characterize these mutations on both *gas-1* G0 and wildtype N2 backgrounds. Among the nine total SNPs discovered within MA431, three affected genes within the *gas-1*-centric interactome: *rheb-1*, *daf-2*, and *sel-2*. All reside on chromosome III separated by approximately: 8.5 cM (*rheb-1* and *daf-2*), 3.5 cM (*rheb-1* and *sel-2*), and 11.0 cM (*daf-2* and *sel-2*) (Wormbase, version WS254), meaning we could expect $\sim 8.5\%$, 3.5% , and 11% of chromatids from each cross to be recombinant for each pair, respectively. Contrary to this expectation, we observed no recombinant genotypes over the course of the seven-generation backcrossing experiment, but our power to detect such genotypes was limited by the small number of offspring ($n = 30\text{--}44$) we could practicably sample and genotype at each generation. We were, however, successful in separating this group of SNPs from all others except one; a fourth SNP on chromosome V remained linked to the chromosome III set. This SNP resided within *C04E12.10* (Wormbase, version WS254), an orthologue of human *NGLY1* (N-glycanase 1)

Table 2
gas-1 MA Line Mutations

<i>gas-1</i> MA Line	Position	Type Conversion	Mutation Type	Gene	Classification	Ref Codon	Ref AA	Var Codon	Var AA	Syn or Non
MA412	II: 11,182,784	A: T → C: G	A → C	F37H8.3	Exon	CCA	Pro	CCC	Pro	Syn
MA412	II: 13,912,231	G: C → A: T	G → A	W02B8.2	Exon	GAG	Glu	AAG	Lys	Non
MA412	V: 11,394,089	A: T → G: C	A → G		Intergenic					
MA412	V: 12,318,251	A: T → C: G	T → G		Intergenic					
MA412	V: 19,920,250	A: T → G: C	A → G		Intergenic					
MA412	V: 20,674,727	G: C → T: A	G → T	<i>mlt-11</i>	Exon	TCG	Ser	TCT	Ser	Non
MA412	X: 5,107,789	A: T → G: C	T → C		Intergenic					
MA412	X: 6,529,937	A: T → G: C	T → C		Intergenic					
MA412	X: 10,265,783	G: C → C: G	G → C		Intergenic					
MA419	III: 896,522	G: C → T: A	G → T	F23H11.2	Exon	TGC	Cys	TTC	Phe	Non
MA419	V: 3,152,259	A: T → T: A	T → A		Intergenic					
MA419	X: 10,274,961	G: C → A: T	C → T	F41E7.2	Intron					
MA419	X: 4,975,182	G: C → C: G	G → C	ZC8.6	Exon	TTC	Phe	TTG	Phe	Syn
MA419	X: 10,368,359	G: C → T: A	G → T		Intergenic					
MA419	X: 12,384,471	G: C → A: T	C → T		Intergenic					
MA429	I: 12,870,206	G: C → A: T	C → T		Intergenic					
MA429	II: 4,663,692	G: C → A: T	C → T	T05A7.11	Exon	GCA	Ala	ACA	Thr	Non
MA429	IV: 3,470,137	G: C → A: T	G → A	F58E2.2	Exon	AAG	Lys	AAA	Lys	Syn
MA429	X: 17,133,019	G: C → A: T	C → T	K09E3.7	Exon	GTG	Vak	ATG	Met	Non
MA429	X: 17,132,998	A: T → G: C	T → C	K09E3.7	Exon	ACA	Thr	GCA	Ala	Non
MA431	I: 10,724,831	A: T → G: C	A → G	<i>srz-85</i>	Exon	CAT	His	CAC	His	Syn
MA431	III: 9,455,062	A: T → T: A	A → T	<i>rheb-1</i>	Intron					
MA431	III: 3,002,544	G: C → T: A	G → T	<i>daf-2</i>	Intron					
MA431	III: 4,598,014	G: C → A: T	C → T	<i>sel-2</i>	Exon	CGT	Arg	CAT	His	Non
MA431	IV: 12,986,492	G: C → A: T	C → T		Intergenic					
MA431	IV: 14,058,054	A: T → T: A	T → A		Intergenic					
MA431	IV: 17,181,972	G: C → A: T	G → A	C52D10.3	Intron					
MA431	V: 3,379,498	G: C → C: G	G → C	C04E12.10	Exon	GAT	Asp	CAT	His	Non
MA431	X: 5,964,400	A: T → T: A	T → A	R07E4.1	Intron					
MA438	I: 8,987,554	G: C → A: T	G → A		Intergenic					
MA438	II: 13,977,894	G: C → A: T	G → A	<i>sre-48</i>	Intron					
MA438	III: 2,792,754	G: C → T: A	G → T	Y71H2AM.24	Intron					
MA438	III: 11,412,255	A: T → C: G	A → C	<i>twk-31</i>	Intron					
MA438	IV: 2,620,955	G: C → A: T	G → A	<i>smf-3</i>	Intron					
MA438	IV: 7,452,889	G: C → A: T	G → A		Intergenic					
MA438	V: 14,423,155	G: C → A: T	C → T		Intergenic					
MA438	V: 1,646,965	A: T → C: G	A → C	<i>alh-2</i>	Exon	TGA	Trp	TGC	Cys	Non
MA438	V: 18,784,124	A: T → G: C	T → C	Y17D7B.10	Intron					
MA438	X: 9,580,008	A: T → T: A	A → T		Intergenic					
MA438	X: 17,456,803	G: C → A: T	G → A		Intergenic					

Ref Allele, reference allele; Var allele, variant allele; Ref Codon, Reference Codon; Ref AA, reference amino acid; Var Codon, variant codon; Var AA, variant amino acid; Syn or Non, synonymous or nonsynonymous mutation.

(Camon 2003; Mulder 2003), resulting in replacement of an asparagine with a histidine.

We found no evidence that the latter observation resulted from a translocation event occurring within either *gas-1* G0 or MA431. To investigate this possibility, de novo assemblies of both the *gas-1* progenitor strain and *gas-1* MA431 were conducted using CLC Genomics Workbench and used to create custom BLAST databases. A 500-bp section of the MA431 chromosome V containing

the SNP (V: 3,379,000–3,379,499 bp) was then used as the BLAST query against both custom BLAST databases. Finally, the top contigs—with 6-kb flanking sequences—returned from each BLAST search were then used as a BLAST query against the N2 reference genome (WS242) with the expectation that, if the chromosome V SNP was both specific to MA431 and not the result of a translocation, the BLAST searches would return only chromosome V sequences. A caveat is that if a segment of highly repetitive DNA joined

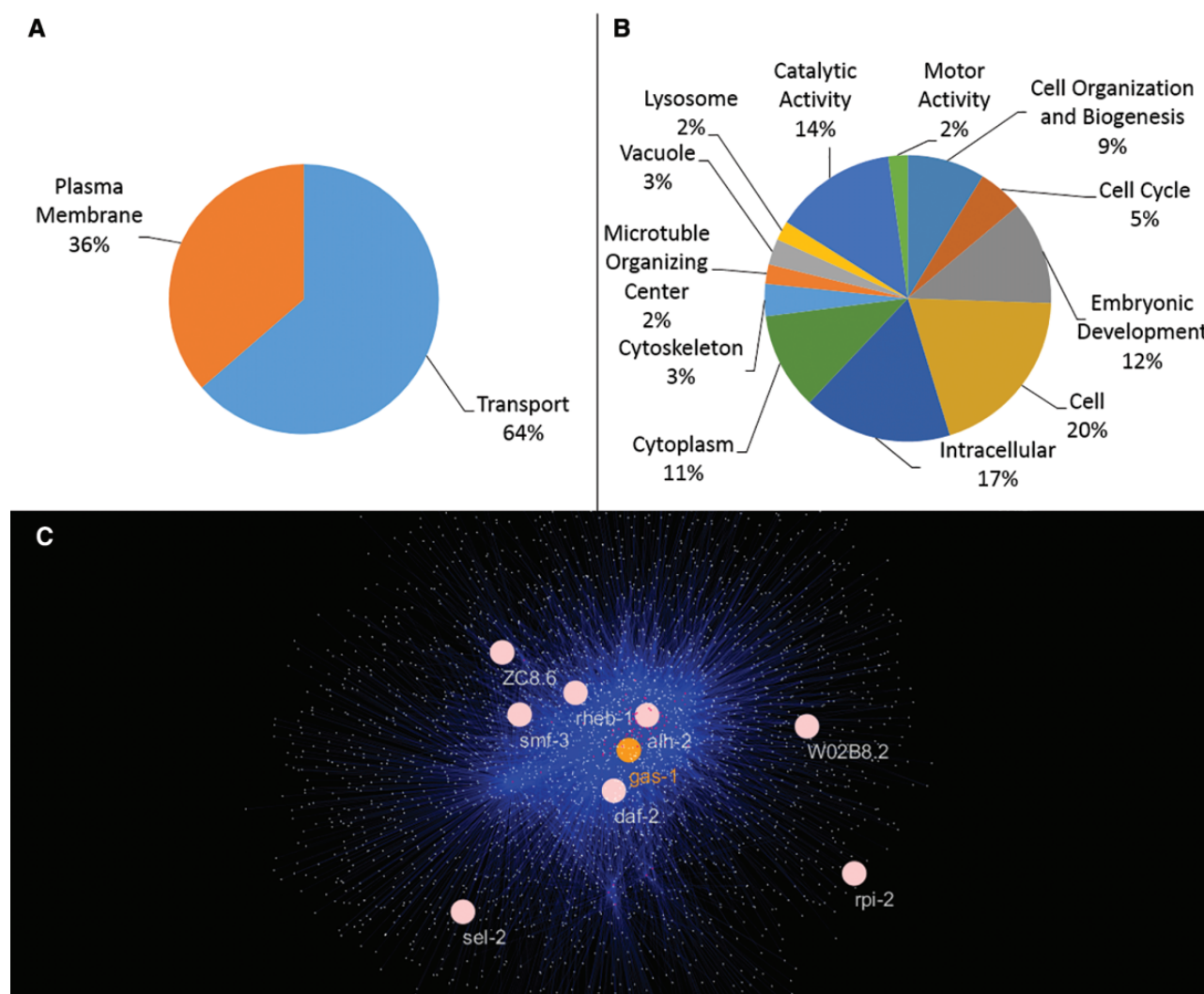


Fig. 3.—GO slim enrichments and *gas-1*-centric interactome. Nonoverlapping sets of GO slims were enriched in *gas-1* (A) and N2 lines (B), which experienced maxima of 47 and 250 generations of mutation accumulation, respectively. (C) Depiction of genes (blue points) predicted to interact within 2-degrees of the *gas-1* gene (orange); genes within this network that acquired mutations in one of the five sequenced *gas-1* MA lines are shown in pink.

the translocated region, the de novo assembly would be unable to construct a contig across that region.

The four isolated MA431 SNPs increased relative fitness on both *gas-1* G0 and wildtype N2 backgrounds (fig. 4), exhibiting a slightly greater selective benefit on the N2 ($s = 0.065$; fig. 4A) compared with the *gas-1* G0 background ($s = 0.029$; fig. 4B). Fitness of the *gas-1* G0 and *gas-1*^{MA431} pair of strains was dramatically reduced compared with the N2 and N2^{MA431} pair (Tukey HSD, $\alpha = 0.05$). This between-pair difference overshadowed the small but significant differences within each pair (fig. 4). The improved fitness of MA431-SNP containing strains was mainly due to increased early life (but not total) reproduction compared with *gas-1* G0 or N2 (supplementary fig. S6 and table S4, Supplementary Material online). Note that N2 “catches up” on the second reproductive day, producing significantly more offspring than N2^{MA431}.

Strains also varied with respect to age-specific survival (supplementary fig. S7, Supplementary Material online) and mortality risk (log-rank $\chi^2_3 = 19.29$, $P < 0.0001$) such that *gas-1*^{MA431} mortality was reduced compared with *gas-1* G0 (risk ratio: 0.546, 95% C.I. = 0.347–0.856, $P < 0.008$), but N2^{MA431} mortality was indistinguishable from that of N2. No differences in average lifespan (mean number of days \pm SEM) were detected among *gas-1*^{MA431} (14.67 ± 0.773), *gas-1* G0 (12.29 ± 0.613), N2^{MA431} (15.80 ± 0.673), or N2 (17.53 ± 0.586).

ROS levels differed among the four experimental strains (supplementary fig. S8, Supplementary Material online; $F_3, 166 = 20.95$, $P < 0.0001$), such that *gas-1*^{MA431} ROS was reduced compared with *gas-1* G0, and both *gas-1* (*fc21*)-containing strains exhibited higher ROS levels than N2 and N2^{MA431} at $P < 0.01$ (Tukey’s HSD, $\alpha = 0.05$). Strains also

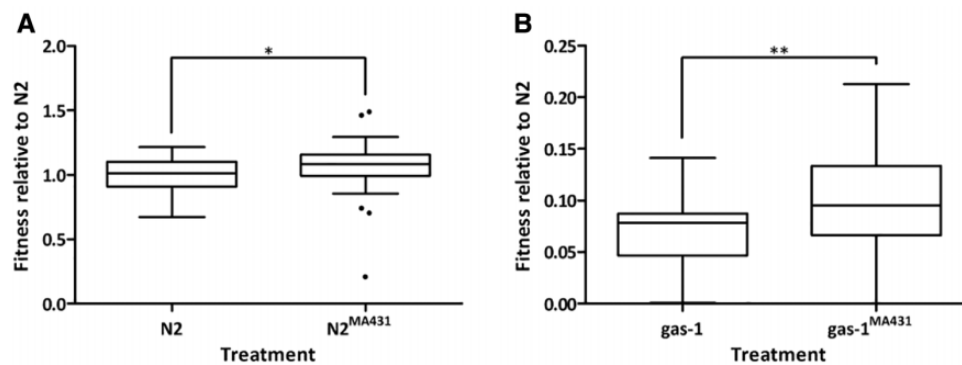


FIG. 4.—Relative fitnesses for MA431 SNP-containing lines and ancestral controls. Fitness of MA431 backcrossed lines relative to N2 reported (mean \pm 1 SEM); note the different y-axis scales in each panel: Wilcoxon rank sums tests showed that N2^{MA431} had improved fitness compared with N2 ($\chi^2_{(1)} = 5.16$, $P < 0.02$) and that *gas-1*^{MA431} had improved fitness compared with *gas-1* G0 ($\chi^2_{(1)} = 7.34$, $P < 0.01$). (A) Wildtype N2 (1.000 ± 0.021) and N2^{MA431} (1.065 ± 0.033) and (B) *gas-1* G0 (0.068 ± 0.005) and *gas-1*^{MA431} (0.097 ± 0.008). * and ** denote statistical significance at $P < 0.01$ and < 0.05 levels, respectively.

varied in their ATP content (supplementary fig. S9, Supplementary Material online; $F_{3, 16} = 9.781$, $P = 0.0007$), such that N2 had significantly higher ATP levels than either of the *gas-1* (*fc21*)-containing strains at $P < 0.01$, and marginally higher levels than N2^{MA431} at $P = 0.0695$ (Tukey's HSD, $\alpha = 0.05$). N2^{MA431}, *gas-1* G0 and *gas-1*^{MA431} ATP levels were statistically indistinguishable.

Discussion

We reported on phenotypic and nuclear genome evolution of *C. elegans* MA lines initiated from a mitochondrial ETC mutant (*gas-1*) compared with previously studied lines initiated from a wildtype (N2) ancestor (Baer et al. 2005). We also functionally characterized a set of mutations that arose during controlled laboratory evolution—the first *C. elegans* experiment to do so.

Genetic Analysis of *gas-1* G0 Reveals Residual Mutations Consistent with EMS Generation

Ideally, MA lines initiated from isogenic strains of *gas-1* (*fc21*) and N2 would be compared with determine how *gas-1* (*fc21*) affects evolution under drift. Because the *gas-1* strain resulted from EMS mutagenesis, we backcrossed it to our laboratory N2 to eliminate extraneous mutations resulting from this treatment, $\sim 99\%$ of which were expected to be G: C \rightarrow A: T transitions (Greene et al. 2003; Kim et al. 2006). Our results were consistent with a swath of EMS-generated mutations having been maintained even after backcrossing due to linkage with the selected *gas-1* (*fc21*) mutation. The original *gas-1* (*fc21*) strain was not sequenced, but we speculate that it contained vastly more EMS-induced mutations than our backcrossed strain. These findings are concerning considering the large number of previous studies employing the CGC *gas-1* (*fc21*)-containing strain and others derived from chemical mutagenesis. In any case, whereas we can safely compare

gas-1 G0 with its resulting MA lines, comparisons of *gas-1* G0 with N2 and between MA lines generated from each strain must be viewed with some caution because we failed to eliminate all genetic differences between the two ancestral strains. Future work targeting single SNPs using CRISPR-Cas9 gene editing can avoid these potential problems.

gas-1 G0 Exhibits Elevated ROS and a “Slow-Living” Phenotype

Keeping the above caveat in mind, *gas-1* G0 was substantially less fit than N2 owing to reduced reproductive output alongside delayed reproductive maturity. As in previous studies (Kayser et al. 2001, 2004), *gas-1* G0 exhibited increased ROS and depressed ATP levels relative to wildtype. We also previously found that pharyngeal pumping rates, a biomarker of age in *C. elegans* (Collins et al. 2008), were much lower in *gas-1* G0 than in N2 and failed to show the typical pattern of age-correlated decline (Lue 2015). These phenotypes make sense in light of previous work showing that, whereas the CGC *gas-1* (*fc21*) mutant exhibits elevated ROS and oxidative stress, it also upregulates expression of numerous metabolic and cellular defence pathways (Falk et al. 2008). The latter is consistent with the fact that DAF-16, the single FOXO transcription factor present in *C. elegans*, is constitutively translocated to nuclei in this mutant, an event that normally occurs only under conditions of starvation, oxidative, and other forms of stress in wildtype nematodes (Kondo et al. 2005). *daf-16* is negatively regulated by the insulin/insulin-like growth factor (IGF) signaling pathway and, in response to environmental stimuli, regulates ~ 100 genes encoding protective products such as heat shock proteins and antioxidants (Hu 2007). The presence of DAF-16 in the nuclei of *gas-1* mutants could result from either or both its high intracellular ROS levels or reduced rates of pharyngeal pumping if the latter leads to dietary restriction, and account for its “slow-living” phenotype (c.f.

Feng et al. 2001). The former scenario seems more likely since *gas-1* worms did not have noticeable frequencies of Dauer larva (personal observation), which might be expected under diet restriction (Hu 2007).

gas-1 nDNA Mutation Spectrum but Not Per-Generation Rate Differs from Wildtype

Oxidative stress is associated with two major base-substitution types; G: C → A: T transitions and G: C → T: A transversions, caused by 5-hydroxyuracil and 8-oxo-dG lesions, respectively (Wiseman and Halliwell 1996; Cooke et al. 2003; Cooke and Evans 2007). Both types were found to predominate the nDNA mutational spectrum in N2 MA lines (Denver et al. 2009); conversely, the *gas-1* mutational spectrum was dominated by G: C → A: T transitions alone. Although this difference could indicate different underlying mechanisms of mutation, considerable evidence from this study indicates that *gas-1* MA line mutations had been filtered by selection. G: C → T: A transversions may therefore have been selectively removed in *gas-1* MA lines. Similarly, our previous analysis of mtDNA mutation within the same lines found that, whereas rates of heritable mtDNA mutation in *gas-1* MA lines were indistinguishable from wildtype, the molecular spectrum of mutations was skewed—in that case toward an increased frequency of single nucleotide substitutions and a reduced frequency of indels compared with wildtype (Wernick et al. 2016). The potentially biased sample of mutations, combined with the downward evolution of ROS levels during *gas-1* MA, makes it impossible to test for a relationship between endogenous ROS and germline mutation rate in this system. Our results are also in general agreement with those of Joyner-Matos et al. (2011) who found that MA lines initiated from a *mev-1* (*kn-1*) ETC complex II mutant, known to experience high endogenous ROS levels (Senoo-Matsuda et al. 2001), exhibited wildtype rates of fitness decay. It is possible that ROS levels decreased during the MA phase in this experiment as well.

Life History and Bioinformatic Results Signal Positive and Purifying Selection in *gas-1* MA Lines

Contrary to results of standard MA studies, after fewer than 50 generations of single-individual bottlenecks, mean absolute, and relative fitness of *gas-1* MA lines improved slightly beyond that of their ancestral *gas-1* G0 control, whereas among-line variance in these traits declined. For comparison, the mutational variance, V_M , for absolute fitness (W) was 5.77 for the N2 MA lines (Baer et al. 2005) compared with a negative estimate, -1.547 , for the *gas-1* MA lines. Improved *gas-1* MA line fitness was entirely due to improvements in early life reproduction beyond that of *gas-1* G0. Because *gas-1* MA lines were initiated from a genetically homogeneous ancestral population and evolved by strict selfing, and since neither reversion of the *gas-1* mutant allele nor loss of the *gas-1*

G0 background mutations was observed in any MA line, their fitness gains were necessarily fuelled by fixation of de novo beneficial or compensatory epistatic mutations. The most likely fate of such mutations arising in this unfavorable population genetic environment would be loss by drift, but the high numbers of failed bottlenecks and *gas-1* MA line extinctions is consistent with selection operating at individual and/or intra-individual (e.g., gametic) levels. Additionally, the increased numbers of nonviable eggs is indicative of purifying selection (e.g., at zygotic or postzygotic levels) against new deleterious mutations, and suggests that an increased fraction of mutations was lethal on the *gas-1* genetic background compared with N2. More work would be required to identify the mechanism(s) of selection in the *gas-1* MA lines, but our findings recall those of the *Arabidopsis thaliana* MA experiments of Shaw and colleagues (Shaw et al. 2000, 2002; Rutter et al. 2010) where mean fitness of wildtype MA lines remained unchanged over generations of inbreeding, a pattern that may have resulted from the action of somatic cell lineage selection occurring in the meristem prior to formation of germ cells (Otto and Orive 1995). Our *gas-1* MA lines may have benefitted from a different form of intraindividual selection that yielded a similar outcome.

Results of our bioinformatics analyses also bore the signature of selection and were consistent with the idea that some *gas-1* MA line mutations conferred beneficial or compensatory effects. First, fewer GO slim categories were significantly enriched in the *gas-1* MA line mutated gene set compared with that of the N2 MA lines. The GoMiner enrichment algorithm takes the total number of altered genes into account when calculating enrichment scores, so this pattern is not a consequence of N2 MA lines having more mutations and is instead consistent with a weaker role for genetic drift in *gas-1* MA versus N2 MA line molecular evolution. Second, four genic mutations in the *gas-1* MA lines—*daf-2*, *rheb-1*, *twk-31*, and *smf-3*—had membership in the same GO slim categories—transport, plasma membrane, and cell (the latter not significantly enriched)—suggesting or confirming known overlap in their function. For instance, *daf-2* (the *C. elegans* insulin/IGF-1 receptor) and *rheb-1* (a GTPase) are known members of the nutrient-sensing target of rapamycin, TOR, pathway that affects growth and longevity; reviewed in Lapierre and Hansen (2012). It may be that altering the transport of nutrients, signaling molecules, or other proteins and ions across membranes counterbalances *gas-1*-associated mitochondrial dysfunction. Given these genes' membership in important metabolic pathways (insulin signaling; mitochondrial unfolded protein response; K^+ transport), it is possible that any ameliorating effects act by altering flux in these pathways at plasma membrane junctions. Third, the number of *gas-1* MA line mutations occurring within *gas-1* interactome genes was higher than expected by chance, suggesting that some *gas-1* MA line mutations were fixed in response to the *gas-1* mutation rather than resulting from drift. Finally, four of

the mutated genes—*daf-2*, *rheb-1*, *smf-3*, and *sel-2*—with membership in the enriched *gas-1* MA GO slim categories (plasma membrane and transport) were also members of the *gas-1* interactome. Interestingly, the plasma membrane category was not significantly enriched among *gas-1* interactome genes, yet they may have been an important target for compensatory or beneficial mutation in the *gas-1* MA lines.

Potential for Protective Metabolic Shift in *gas-1* MA Lines

The evolution of *gas-1* MA ROS levels toward lower, wildtype levels contrasts with the elevated ROS levels we previously observed among N2 MA lines (Joyner-Matos et al. 2013). Conversely, the MA process had little impact on steady-state ATP levels in *gas-1* MA lines—the same was true for pharyngeal pumping (Lue 2015). A potential explanation for these combined results is that the *gas-1* MA lines benefitted from a metabolic shift toward increased reliance upon fermentation and away from oxidative phosphorylation—a phenomenon known to occur in certain cancer cells (the Warburg effect, Warburg 1956). By utilizing one or more of their diverse fermentation pathways (Holt and Riddle 2003; Hulme and Whitesides 2011), *C. elegans* could reduce mitochondrial ROS production, perhaps offsetting the cost of the strain's already low ATP (Tielens et al. 2002), preventing apoptosis (Ruckenstuhl et al. 2009), or increasing mtDNA genome stability (Ericson et al. 2012). In the absence of gene expression or other supporting data, we do not know whether such a shift, if one occurred, resulted from fixation of beneficial mutations and/or a stress response to deleterious MA in *gas-1* MA lines.

Beneficial Haplotype Characterization Indicates Role for Epistasis

Although we were unable to isolate single, candidate beneficial *gas-1* MA431 SNPs to ascertain their individual contributions to the line's slight fitness recovery, this failure revealed a potentially large role for epistasis in *gas-1* MA line fitness evolution. Our inability to break up the three chromosome III SNPs may have been due to their strong linkage and our limited power to detect recombinant genotypes. But failure to isolate the chromosome V SNP from the chromosome III group is consistent with some form of epistasis operating between this SNP and one or more on chromosome III. Interestingly, the four-SNP combination proved to be slightly more advantageous on its nonnative N2 background, and thus did not appear to specifically compensate for the *gas-1* (*fc21*) mutation. This result was somewhat surprising given the interactome results and the reasonable expectation that N2 had achieved maximal laboratory adaptation, and is consistent with the existence of a rugged genetic landscape in which a new local fitness peak was opened to N2 by addition of the MA431 SNP set (c.f., Poelwijk et al. 2007). Two genetic explanations for this outcome include one of strong positive

epistasis operating between some combination of MA431 SNPs, which would be neutral or beneficial on their own but advantageous in combination (Phillips 2008); in this scenario, the MA431 SNPs could have conferred a greater advantage on the N2 background simply because they did not have to contend with the 76 background mutations present within *gas-1* GO. A second possibility is one of reciprocal sign epistasis (Kvitek and Sherlock 2011; Poelwijk et al. 2011), in this case involving individually deleterious mutations conferring a beneficial effect in combination. As previously noted, when any one of four MA431 SNPs was lost during the backcrossing phase, all others would be lost in the following generation—an outcome consistent with this form of epistasis operating between some combination of SNPs. If true, the mutational route to this beneficial SNP combination may have been complex given the likely existence of low-fitness intermediate genotypes; a transgenerational analysis of *gas-1* MA431 mutational dynamics would be necessary to distinguish among these possibilities.

In contrast to the similar fitness effects of the MA431 SNPs in the *gas-1* GO versus N2 strains, their physiological effects were strongly strain-dependent. The four SNPs' *gas-1* GO-specific consequences (reduced ROS levels with no effect on ATP levels) are consistent with our metabolic shift hypothesis (above), whereas the consequences for N2 (reduced ATP levels with no effect on ROS levels) are more mysterious. Clearly, more work would be required to fully characterize the MA431 SNP set, but these results reveal strong context-dependency in its effects at the physiological level. Finally, we note that the above interpretations ignore the possibility of epistatic interactions between the MA431 SNP set and mtDNA variants and/or nDNA mutation types not considered here. The former at least seems unlikely since, although we previously identified four heteroplasmic mtDNA variants segregating within the MA431 line, none were detected at levels exceeding ~4% in the sampled population (table 4 in Wernick et al. 2016).

Conclusion

Our study indicates that, even under conditions of extreme genetic drift, low-fitness populations can maintain or slightly improve their fitness through both selective elimination of deleterious mutations and fixation of novel beneficial mutations or allelic combinations. These unusual results are consistent with predictions of adaptive landscape theory—namely, with the existence of an inverse relationship between a population's fitness and its likelihood of adaptation, and considerable context dependency of the mutational distribution of fitness effects. A greater fraction of new mutations may confer beneficial and lethal effects in populations existing at low-fitness extremes, simultaneously opening more mutational routes to both fitness maintenance/recovery and extinction. In addition, the fact that we observed only minor fitness

improvements—nothing approaching complete recovery of ancestral fitness levels—in *gas-1* MA lines is consistent with the prediction that most advantageous mutations confer only small fitness benefits; however, the individual effects of any medium- or large-effect beneficial mutations acquired by the *gas-1* MA lines were likely muted by deleterious mutations present in the same genomes. The above interpretation was supported by our bioinformatic analyses, which revealed highly nonrandom patterns of genetic network location and functional annotation among *gas-1* versus N2 MA line mutations. Interestingly, these analyses implicated some of the same pathways known to be upregulated in the *gas-1* mutant ancestor (Falk et al. 2008), suggesting that both genetic and nongenetic responses may tend to occur via similar or overlapping pathways. This study also revealed the capacity of ETC-deficient populations experiencing relaxed selection to rapidly recover near-wildtype levels of ROS—a pattern that may have been at least partly due to nongenetic mechanisms (i.e., compensatory transcriptional upregulation of metabolic and damage response pathways, Falk et al. 2008), which were further activated in response to deleterious MA in the *gas-1* background. The downward evolution of ROS levels was accompanied by maintenance of a wildtype mutation rate but an altered mutational spectrum—a result similar to that of our previous analysis of mtDNA mutation processes in the same lines (Wernick et al. 2016). Understanding the extent to which this pattern may be due to selection favoring or eradicating particular base-substitution types would require further study. Lastly, our characterization of a SNP combination fixed within one *gas-1* MA line was consistent with a role for reciprocal sign epistasis in fitness evolution in our system, and adds to the growing body of evidence that fitness landscapes are rugged and, whereas possibly dominated by genetic constraint, can provide routes to adaptation and “accessible innovation” (c.f., fig. 3 in Barrick and Lenski 2013).

Supplementary Material

Supplementary data are available at *Genome Biology and Evolution* online.

Acknowledgments

We thank B. Taylor, J. Podrabsky and T. Rosenstiel for helpful discussion; and A. Basler, A. Coleman-Hulbert, L. Munoz-Tremblay, A. Mustain, and J. Sullins for laboratory support; and anonymous reviewers for thoughtful comments on the manuscript. This work was supported the National Science Foundation [MCB-1330427 to S.E. and D.R.D., and HRD-140465, which supported the undergraduate research of G.V.]; and the PSU Biology Department [Forbes-Lea grant to S.F.C.]. We also thank the OSU Center for Genome Research

and Biocomputing for DNA sequencing and bioinformatics support.

Literature Cited

- Achaz G, et al. editors. 2014. Ecological genomics: ecology and the evolution of genes and genomes. Netherlands: Springer. p. 211–231.
- Ameur A, et al. 2011. Ultra-deep sequencing of mouse mitochondrial DNA: mutational patterns and their origins. *PLoS Genet.* 7(3):e1002028.
- Andrew JR, et al. 2015. Abiotic stress does not magnify the deleterious effects of spontaneous mutations. *Heredity* 115:503–508.
- Baer CF, et al. 2005. Comparative evolutionary genetics of spontaneous mutations affecting fitness in rhabditid nematodes. *Proc Natl Acad Sci U S A.* 102:5785–5790.
- Barrick JE, Kauth MR, Strelieff CC, Lenski RE. 2010. *Escherichia coli* rpoB mutants have increased evolvability in proportion to their fitness defects. *Mol Biol Evol.* 27(6):1338–1347.
- Barrick JE, Lenski RE. 2013. Genome dynamics during experimental evolution. *Nat Rev Genet.* 14(12):827–839.
- Blier PU, Dufresne F, Burton RS. 2001. Natural selection and the evolution of mtDNA-encoded peptides: evidence for intergenomic co-adaptation. *Trends Genet.* 17(7):400–406.
- Burch CL, Chao L. 1999. Evolution by small steps and rugged landscapes in the RNA virus phi6. *Genetics* 151(3):921–927.
- Campan E. 2003. The gene ontology annotation (GOA) project: Implementation of GO in SWISS-PROT, TrEMBL, and InterPro. *Genome Res.* 13:662–672.
- Chevin L-M, Martin G, Lenormand T. 2010. Fisher’s model and the genomics of adaptation: restricted pleiotropy, heterogeneous mutation, and parallel evolution. *Evolution* 64(11):3213–3231.
- Collins JJ, Huang C, Hughes S, Kornfeld K. 2008. The measurement and analysis of age-related changes in *Caenorhabditis elegans*. *WormBook*. p. 1–21.
- Cooke MS, Evans MD. 2007. 8-oxo-deoxyguanosine: reduce, reuse, recycle? *Proc Natl Acad Sci U S A.* 104(34):13535–13536.
- Cooke MS, Evans MD, Dizdaroglu M, Lunec J. 2003. Oxidative DNA damage: mechanisms, mutation, and disease. *FASEB J.* 17(10):1195–1214.
- Demple B, Harrison L. 1994. Repair of oxidative damage to DNA: enzymology and biology. *Annu Rev Biochem.* 63:915–948.
- Denver DR, et al. 2009. A genome-wide view of *Caenorhabditis elegans* base-substitution mutation processes. *Proc Natl Acad Sci U S A.* 106(38):16310–16314.
- Denver DR, et al. 2010. Selective sweeps and parallel mutation in the adaptive recovery from deleterious mutation in *Caenorhabditis elegans*. *Genome Res.* 20(12):1663–1671.
- Denver DR, et al. 2012. Variation in base-substitution mutation in experimental and natural lineages of *Caenorhabditis nematodes*. *Genome Biol Evol.* 4(4):513–522.
- Denver DR, Feinberg S, Steding C, Durbin M, Lynch M. 2006. The relative roles of three DNA repair pathways in preventing *Caenorhabditis elegans* mutation accumulation. *Genetics* 174(1):57–65.
- Denver DR, Morris K, Lynch M, Thomas WK. 2004. High mutation rate and predominance of insertions in the *Caenorhabditis elegans* nuclear genome. *Nature* 430:679–682.
- Dowling DK, Friberg U, Lindell J. 2008. Evolutionary implications of non-neutral mitochondrial genetic variation. *Trends Ecol. Evol.* 23(10):546–554.
- Elena SF, Lenski RE. 2001. Epistasis between new mutations and genetic background and a test of genetic canalization. *Evolution* 55:1746–1752.
- Ericson NG, et al. 2012. Decreased mitochondrial DNA mutagenesis in human colorectal cancer. *PLoS Genet.* 8(6):e1002689.

- Estes S, Lynch M. 2003. Rapid fitness recovery in mutationally degraded lines of *Caenorhabditis elegans* rapid fitness recovery in mutationally degraded lines of *Caenorhabditis elegans*. *Evolution* 57(5):1022–1030.
- Estes S, Phillips PC, Denver DR, Thomas WK, Lynch M. 2004. Mutation accumulation in populations of varying size: the distribution of mutational effects for fitness correlates in *Caenorhabditis elegans*. *Genetics* 166(3):1269–1279.
- Falk MJ, et al. 2008. Metabolic pathway profiling of mitochondrial respiratory chain mutants in *C. elegans*. *Mol Genet Metab*. 93(4):388–397.
- Feng J, Bussi ere F, Hekimi S. 2001. Mitochondrial electron transport is a key determinant of life span in *Caenorhabditis elegans*. *Dev Cell* 1(5):633–644.
- Fisher R. 1930. On the genetical theory of natural selection. Oxford (United Kingdom): Oxford University Press.
- Greene EA, et al. 2003. Spectrum of chemically induced mutations from a large-scale reverse-genetic screen in *Arabidopsis*. *Genetics* 164(2):731–740.
- Hall DW, Mahmoudzad R, Hurd AW, Joseph SB. 2008. Spontaneous mutations in diploid *Saccharomyces cerevisiae*: another thousand cell generations. *Genet Res*. 90(3):229–241.
- Halligan DL, Keightley PD. 2009. Spontaneous mutation accumulation studies in evolutionary genetics. *Annu Rev Ecol Evol Syst*. 40(1):151–172.
- Hartman PS, Ishii N, Kayser E-B, Morgan PG, Sedensky MM. 2001. Mitochondrial mutations differentially affect aging, mutability and anesthetic sensitivity in *Caenorhabditis elegans*. *Mech Ageing Dev*. 122(11):1187–1201.
- Heilbron K, Toll-Riera M, Kojadinovic M, MacLean RC. 2014. Fitness is strongly influenced by rare mutations of large effect in a microbial mutation accumulation experiment. *Genetics* 197(3):981–990.
- Hicks KA, Howe DK, Leung A, Denver DR, Estes S. 2012. In vivo quantification reveals extensive natural variation in mitochondrial form and function in *Caenorhabditis briggsae*. *PLoS ONE* 7(8):e43837.
- Hietpas RT, Bank C, Jensen JD, Bolon DNA. 2013. Shifting fitness landscapes in response to altered environments. *Evolution* 67(12):3512–3522.
- Holt SJ, Riddle DL. 2003. Sage surveys *C. elegans* carbohydrate metabolism: evidence for an anaerobic shift in the long-lived dauer larva. *Mech Ageing Dev*. 124(7):779–800.
- Hsie AW, et al. 1986. Evidence for reactive oxygen species inducing mutations in mammalian cells. *Proc Natl Acad Sci U S A*. 83(24):9616–9620.
- Hu PJ. 2007. Dauer. *WormBook*. p. 1–19.
- Hu Z-L, Bao J, Reecy JM. 2008. CateGORizer: a web-based program to batch analyze gene on-tology classification categories. *Online J Bioinform*. 9:108–112.
- Hulme SE, Whitesides GM. 2011. Chemistry and the worm: *Caenorhabditis elegans* as a platform for integrating chemical and biological research. *Angew Chem Int Ed*. 42(35):4774–4807.
- Itsara LS, et al. 2014. Oxidative stress is not a major contributor to somatic mitochondrial DNA mutations. *PLoS Genet*. 10(2):e1003974.
- Joseph SB, Hall DW. 2004. Spontaneous mutations in diploid *Saccharomyces cerevisiae*: more beneficial than expected. *Genetics* 168(4):1817–1825.
- Joyner-Matos J, Bean LC, Richardson HL, Sammel T, Baer CF. 2011. No evidence of elevated germline mutation accumulation under oxidative stress in *Caenorhabditis elegans*. *Genetics* 189(4):1439–1447.
- Joyner-Matos J, et al. 2013. Evolution of a higher intracellular oxidizing environment in *Caenorhabditis elegans* under relaxed selection. *PLoS One* 8(6):4–9.
- Katju V, Packard LB, Bu L, Keightley PD, Bergthorsson U. 2015. Fitness decline in spontaneous mutation accumulation lines of *Caenorhabditis elegans* with varying effective population sizes. *Evolution* 69(1):104–116.
- Kayser EB, Morgan PG, Hoppel CL, Sedensky MM. 2001. Mitochondrial expression and function of GAS-1 in *Caenorhabditis elegans*. *J Biol Chem*. 276(23):20551–20558.
- Kayser EB, Morgan PG, Sedensky MM. 1999. GAS-1: a mitochondrial protein controls sensitivity to volatile anesthetics in the nematode *Caenorhabditis elegans*. *Anesthesiology* 90(2):545–554.
- Kayser EB, Sedensky MM, Morgan PG. 2004. The effects of complex I function and oxidative damage on lifespan and anesthetic sensitivity in *Caenorhabditis elegans*. *Mech Ageing Dev*. 125(6):455–464.
- Keightley PD, et al. 2009. Analysis of the genome sequences of three *Drosophila melanogaster* spontaneous mutation accumulation lines analysis of the genome sequences of three *Drosophila melanogaster* spontaneous mutation accumulation lines. *Genome Res*. 19(7):1195–1201.
- Kim Y, Schumaker K, Zhu J-K. 2006. EMS mutagenesis of *Arabidopsis*. *Methods Mol Biol*. 323:101–103.
- Kondo M, et al. 2005. Effect of oxidative stress on translocation of daf-16 in oxygen-sensitive mutants, mev-1 and gas-1 of *Caenorhabditis elegans*. *Mech Ageing Dev*. 126(6–7):637–641.
- Kondrashov FA, Kondrashov AS. 2010. Measurements of spontaneous rates of mutations in the recent past and the near future. *Philos Trans R Soc B Biol Sci*. 365(1544):1169–1176.
- Kvitek DJ, Sherlock G. 2011. Reciprocal sign epistasis between frequently experimentally evolved adaptive mutations causes a rugged fitness landscape. *PLoS Genetics* 7(4):e1002056.
- Lande R. 1994. Risk of population extinction from fixation of new deleterious mutations. *Evolution* 48(5):1460–1469.
- Lapierre LR, Hansen M. 2012. Lessons from *C. elegans*: signaling pathways for longevity. *Trends Endocrinol Metab*. 23(12):637–644.
- Lee H, Popodi E, Tang H, Foster PL. 2012. Rate and molecular spectrum of spontaneous mutations in the bacterium *Escherichia coli* as determined by whole-genome sequencing. *Proc Natl Acad Sci U S A*. 109(41):E2774–E2783.
- Lenaz G, et al. 2006. Mitochondrial complex I: structural and functional aspects. *Biochim Biophys Acta* 1757(9–10):1406–1420.
- Lenski RE, Travisano M. 1994. Dynamics of adaptation and diversification: a 10,000-generation experiment with bacterial populations. *Proc Natl Acad Sci U S A*. 91(15):6808–6814.
- Lue M. 2015. Phenotypic and mutational consequences of mitochondrial ETC genetic damage [thesis]. [Portland (OR)]: Portland State University.
- Lynch M, B urger R, Butcher D, Gabriel W. 1993. The mutational meltdown in asexual populations. *J Hered*. 84(5):339–344.
- Lynch M, Conery J, Burger R. 1995. Mutation accumulation and the extinction of small populations. *Am Nat*. 146(4):489–518.
- Lynch M, et al. 1999. Perspective: spontaneous deleterious mutations. *Evolution* 53(3):645–663.
- Lynch M, et al. 2008. A genome-wide view of the spectrum of spontaneous mutations in yeast. *Proc Natl Acad Sci U S A*. 105(27):9272–9277.
- Maisnier-Patin S, Berg OG, Liljas L, Andersson DI. 2002. Compensatory adaptation to the deleterious effect of antibiotic resistance in *Salmonella typhimurium*. *Mol Microbiol*. 46(2):355–366.
- Martin G, Lenormand T. 2006. A general multivariate extension of Fisher’s geometrical model and the distribution of mutation fitness effects across species. *Evolution* 60(5):893–907.
- Martin G, Lenormand T. 2015. The fitness effect of mutations across environments: Fisher’s geometrical model with multiple optima. *Evolution* 69(6):1433–1447.
- Miller CR, Joyce P, Wichman HA. 2011. Mutational effects and population dynamics during viral adaptation challenge current models. *Genetics* 187(1):185–202.
- Mittler R, et al. 2011. ROS signaling: the new wave? *Trends Plant Sci*. 16(6):300–309.

- Morgan PG, Sedensky MM. 1994. Mutations conferring new patterns of sensitivity to volatile anesthetics in *Caenorhabditis elegans*. *Anesthesiology* 81(4):888–898.
- Mulder NJ. 2003. The InterPro database, 2003 brings increased coverage and new features. *Nucleic Acids Res.* 31:315–318.
- Murphy MP. 2009. How mitochondria produce reactive oxygen species. *Biochem J.* 417(1):1–13.
- Orr HA. 1998. The population genetics of adaptation: the distribution of factors fixed during adaptive evolution. *Evolution* 52(4):935–949.
- Orr HA. 2000. Adaptation and the cost of complexity. *Evolution* 54:13–20.
- Ossowski S, et al. 2010. The rate and molecular spectrum of spontaneous mutations in *Arabidopsis thaliana*. *Science* 327(5961):92–94.
- Otto SP, Orive ME. 1995. Evolutionary consequences of mutation and selection within an individual. *Genetics* 141(3):1173–1187.
- Perfeito L, Fernandes L, Mota C, Gordo I. 2007. Adaptive mutations in bacteria: high rate and small effects. *Science* 317(5839):813–815.
- Poelwijk FJ, Kiviet DJ, Weinreich DM, Tans SJ. 2007. Empirical fitness landscapes reveal accessible evolutionary paths. *Nature* 445(7126):383–386.
- Poelwijk FJ, Tănase-Nicola S, Kiviet DJ, Tans SJ. 2011. Reciprocal sign epistasis is a necessary condition for multi-peaked fitness landscapes. *Journal of Theoretical Biology* 272(1):141–144.
- Poon A, Otto SP. 2000. Compensating for our load of mutations: freezing the meltdown of small populations. *Evolution* 54(5):1467–1479.
- Phillips PC. 2008. Epistasis — the essential role of gene interactions in the structure and evolution of genetic systems. *Nat Rev Genet.* 9:855–867.
- Remold SK, Lenski RE. 2004. Pervasive joint influence of epistasis and plasticity on mutational effects in *Escherichia coli*. *Nat Genet.* 36(4):423–426.
- Rokyta D, Badgett MR, Molineux IJ, Bull JJ. 2002. Experimental genomic evolution: extensive compensation for loss of DNA ligase activity in a virus. *Mol Biol Evol.* 19(3):230–238.
- Ruckenstuhl C, et al. 2009. The Warburg effect suppresses oxidative stress induced apoptosis in a yeast model for cancer. *PLoS One* 4(2):e4592.
- Rutter MT, et al. 2012. Fitness of *Arabidopsis thaliana* mutation accumulation lines whose spontaneous mutations are known. *Evolution* 66(7):2335–2339.
- Rutter MT, Shaw FH, Fenster CB. 2010. Spontaneous mutation parameters for *Arabidopsis thaliana* measured in the wild. *Evolution* 64(6):1825–1835.
- Sanjuan R, Moya A, Elena SF. 2004. The distribution of fitness effects caused by single-nucleotide substitutions in an RNA virus. *Proc Natl Acad Sci U S A.* 101(22):8396–8401.
- Saxer G, et al. 2012. Whole genome sequencing of mutation accumulation lines reveals a low mutation rate in the social amoeba *Dictyostelium discoideum*. *PLoS One* 7(10):e46759.
- Senoo-Matsuda N, et al. 2001. A defect in the cytochrome b large subunit in complex ii causes both superoxide anion overproduction and abnormal energy metabolism in *Caenorhabditis elegans*. *J Biol Chem.* 276:41553–41558.
- Sharp NP, Agrawal AF. 2012. Evidence for elevated mutation rates in low-quality genotypes. *Proc Natl Acad Sci U S A.* 109:6142–6146.
- Shaw FH, Geyer CJ, Shaw RG. 2002. A comprehensive model of mutations affecting fitness and inferences for *Arabidopsis thaliana*. *Evolution* 56(3):453–463.
- Shaw RG, Byers DL, Darmo E. 2000. Spontaneous mutational effects on reproductive traits of *Arabidopsis thaliana*. *Genetics* 155(1):369–378.
- Silander OK, Tenaillon O, Chao L. 2007. Understanding the evolutionary fate of finite populations: the dynamics of mutational effects. *PLoS Biol.* 5(4):e94.
- Smith SW, Latta LC, Denver DR, Estes S. 2014. Endogenous ROS levels in *C. elegans* under exogenous stress support revision of oxidative stress theory of life-history tradeoffs. *BMC Evol Biol.* 14:161.
- Stearns FW, Fenster CB. 2016. The effect of induced mutations on quantitative traits in *Arabidopsis thaliana*: natural versus artificial conditions. *Ecol Evol.* 6(23):8366–8374.
- Tenaillon O. 2014. The utility of Fisher's geometric model in evolutionary genetics. *Annu Rev Ecol Evol Syst.* 45:179–201.
- Teotónio H, Estes S, Phillips PC, Baer CF. 2017. Experimental evolution with *Caenorhabditis nematodes*. *Genetics* 206(2):691–716.
- Tielens AGM, Rotte C, Van Hellemond JJ, Martin W. 2002. Mitochondria as we don't know them. *Trends Biochem Sci.* 27(11):564–572.
- Tong T, Zhao H. 2008. Practical guidelines for assessing power and false discovery rate for a fixed sample size in microarray experiments. *Stat Med.* 27(11):1960–1972.
- Van Raamsdonk JM, et al. 2010. Decreased energy metabolism extends life span in *Caenorhabditis elegans* without reducing oxidative damage. *Genetics* 185(2):559–571.
- Vassilieva LL, Hook AM, Lynch M. 2000. The fitness effects of spontaneous mutations in *Caenorhabditis elegans*. *Evolution* 54(4):1234–1246.
- Wang AD, et al. 2009. Selection, epistasis, and parent-of-origin effects on deleterious mutations across environments in *Drosophila melanogaster*. *Am Nat.* 174(6):863–874.
- Wang Y, Arenas CD, Stoebel DM, Cooper TF. 2013. Genetic background affects epistatic interactions between two beneficial mutations. *Biol Lett.* 9(1):20120328.
- Warburg O. 1956. On the origin of cancer cells. *Science* 123(3191):309–314.
- Wernick RI, Estes S, Howe DK, Denver DR. 2016. Paths of heritable mitochondrial DNA mutation and heteroplasmy in reference and gas-1 strains of *Caenorhabditis elegans*. *Front Genet.* 7:1–12.
- Whitlock MC, Otto SP. 1999. The panda and the phage: compensatory mutations and the persistence of small populations. *Trends Ecol Evol.* 14(8):295–296.
- Wiseman H, Halliwell B. 1996. Damage to DNA by reactive oxygen and nitrogen species: role in inflammatory disease and progression to cancer. *Biochem J.* 313(1):17–29.
- Yang H, Hekimi S. 2010. A mitochondrial superoxide signal triggers increased longevity in *Caenorhabditis elegans*. *PLoS Biology* 8(2):e1000556.
- Yu E, et al. 2013. Mitochondrial DNA damage can promote atherosclerosis independently of reactive oxygen species through effects on smooth muscle cells and monocytes and correlates with higher-risk plaques in humans. *Circulation* 128(7):702–712.
- Zeeberg BR, et al. 2003. Gominer: a resource for biological interpretation of genomic and proteomic data. *Genome Biol.* 4(4):R28.
- Zeeberg BR, et al. 2005. High-Throughput GoMiner, an 'industrial-strength' integrative gene ontology tool for interpretation of multiple-microarray experiments, with application to studies of Common Variable Immune Deficiency (CVID). *BMC Bioinformatics* 6:168.
- Zhong W, Sternberg P. 2006. Genome-wide prediction of *c. elegans* genetic interactions. *Science* 311(5766):1481–1484.

Associate editor: Daniel Sloan